Seasonal Variations of Soil Thermal Conductivity at the InSight Landing Site

M. Grott, S. Piqueux, T. Spohn, J. Knollenberg, C. Krause, E. Marteau, T. L. Hudson, F. Forget, L. Lange, N. Müller, et al.

Geophysical Research Letters

RESEARCH LETTER
10.1029/2023GL102975

Seasonal Variations of Soil Thermal Conductivity at the InSight Landing Site

M. Grott[1], S. Piqueux[2], T. Spohn[1,3], J. Knollenberg[1], C. Krause[4], E. Marteau[2], T. L. Hudson[2], F. Forget[5], L. Lange[5], N. Müller[1], M. Golombek[2], S. Nagihara[6], P. Morgan[7], J. P. Murphy[8], M. Siegler[9,10], S. D. King[8], D. Banfield[11], S. E. Smrekar[2], and W. B. Banerdt[2]

[1]German Aerospace Center (DLR), Institute of Planetary Research, Berlin, Germany, [2]Jet Propulsion Laboratory, California Institute of Technology, Pasadena, CA, USA, [3]International Space Science Institute (ISSI), Bern, Switzerland, [4]German Aerospace Center (DLR), MUSC Space Operations and Astronaut Training, Cologne, Germany, [5]Laboratoire de Météorologie Dynamique (LMD/IPSL/CNRS), Sorbonne Université, Paris, France, [6]Department of Geosciences, Texas Tech University, Lubbock, TX, USA, [7]Colorado Geological Survey, Colorado School of Mines, Golden, CO, USA, [8]Virginia Polytechnic Institute and State University, Blacksburg, VA, USA, [9]Planetary Science Institute, Tucson, AZ, USA, [10]Southern Methodist University, Dallas, TX, USA, [11]Cornell University, Ithaca, NY, USA

Abstract The heat flow and physical properties package measured soil thermal conductivity at the landing site in the 0.03–0.37 m depth range. Six measurements spanning solar longitudes from 8.0° to 210.0° were made and atmospheric pressure at the site was simultaneously measured using InSight's Pressure Sensor. We find that soil thermal conductivity strongly correlates with atmospheric pressure. This trend is compatible with predictions of the pressure dependence of thermal conductivity for unconsolidated soils under martian atmospheric conditions, indicating that heat transport through the pore filling gas is a major contributor to the total heat transport. Therefore, any cementation or induration of the soil sampled by the experiments must be minimal and soil surrounding the mole at depths below the duricrust is likely unconsolidated. Thermal conductivity data presented here are the first direct evidence that the atmosphere interacts with the top most meter of material on Mars.

Plain Language Summary A soil's ability to transport heat is a fundamental parameter that holds information on quantities like soil bulk porosity, composition, grain size, and the state of cementation or induration. In the soil, heat is transported through grain-to-grain contacts as well as through the pore filling CO_2 gas. The heat flow and physical properties package (HP^3) of the InSight Mars mission measured soil thermal conductivity at the landing site repeatedly over the course of a martian year. As atmospheric pressure changes between seasons due to the redistribution of CO_2 across the planet, we found that soil thermal conductivity also changes. Thermal conductivity increased for increased atmospheric pressure, a behavior typical for unconsolidated material. This implies that the amount of cement or induration of the sampled soil must be minimal.

Key Points:

- We measured thermal conductivity of the martian soil and found that its conductivity strongly correlates with atmospheric pressure
- We conclude that heat conduction through the pore-filling gas is significant and that cementation of the soil must be minimal
- Our data show that the atmosphere directly interacts with the top most meter of material on Mars

Supporting Information:

Supporting Information may be found in the online version of this article.

Correspondence to:

M. Grott,
matthias.grott@dlr.de

Citation:

Grott, M., Piqueux, S., Spohn, T., Knollenberg, J., Krause, C., Marteau, E., et al. (2023). Seasonal variations of soil thermal conductivity at the InSight landing site. *Geophysical Research Letters*, *50*, e2023GL102975. https://doi.org/10.1029/2023GL102975

Received 21 JAN 2023
Accepted 27 MAR 2023

Author Contributions:

Conceptualization: M. Grott, P. Morgan
Data curation: M. Grott, F. Forget
Formal analysis: M. Grott, F. Forget, J. P. Murphy
Funding acquisition: M. Grott, T. Spohn, S. E. Smrekar, W. B. Banerdt
Investigation: M. Grott, J. Knollenberg, L. Lange, M. Golombek, P. Morgan
Methodology: M. Grott, J. Knollenberg, T. L. Hudson, F. Forget, L. Lange, N. Müller, P. Morgan, J. P. Murphy, S. D. King
Project Administration: M. Grott
Resources: M. Grott, S. E. Smrekar
Software: M. Grott, L. Lange, P. Morgan, J. P. Murphy
Supervision: S. D. King

1. Introduction

Thermal conductivity is a fundamental physical property that largely controls the range of temperatures experienced at the surface and in the shallow subsurface of a planet. In granular material, heat is transported through grain-to-grain contacts, conduction through the pore-filling gas, and radiation between individual grains. In martian soil, the first two contributions dominate the transport, and grain-to-grain contacts are particularly enhanced if grains are cemented or indurated (Piqueux & Christensen, 2009b; Presley et al., 2009). Conversely, the contribution of heat transport through the gas phase can inform us about the state of soil cementation or induration. Here, the term cementation refers to the deposition of crystalline material and the formation of bridges between grains. In contrast, cohesion is related to an increase in shear strength caused by electrostatic forces. In the following, we will refer to low cohesion granular material as unconsolidated.

For grain sizes between a few μm and a few mm (Edgett et al., 2013; Fergason et al., 2006; Hamilton et al., 2014; Pike et al., 2011; Presley & Christensen, 1997; Yingst et al., 2013) and atmospheric pressures of a few mbar typically encountered on Mars, the mean free path of gas molecules is similar to pore size and gas flow occurs in the transitional flow regime (Piqueux & Christensen, 2009a). This results in a strong dependence of soil thermal conductivity on atmospheric pressure (Huetter et al., 2008; Nagihara et al., 2022; Presley & Christensen, 1997)

Validation: M. Grott, L. Lange, J. P. Murphy, S. D. King
Visualization: M. Grott
Writing – original draft: M. Grott, S. Piqueux, T. Spohn, J. Knollenberg, E. Marteau, T. L. Hudson, F. Forget, L. Lange, N. Müller, M. Golombek, P. Morgan, J. P. Murphy, S. D. King, D. Banfield, S. E. Smrekar, W. B. Banerdt
Writing – review & editing: M. Grott, S. Piqueux, T. Spohn, J. Knollenberg, C. Krause, E. Marteau, T. L. Hudson, F. Forget, L. Lange, N. Müller, M. Golombek, P. Morgan, J. P. Murphy, S. D. King, D. Banfield, S. E. Smrekar, W. B. Banerdt

in unconsolidated material, whereas conduction through the gas phase becomes less important when the soil is cemented or indurated, where conduction mainly occurs through the soil matrix (Piqueux & Christensen, 2009b).

The only in situ thermal measurements of the martian soil using transient heating methods were performed by the thermal and electrical permittivity probe (TECP) during the Phoenix mission (Zent et al., 2010) and those taken by the heat flow and physical properties package (HP^3) on the InSight mission (Banerdt et al., 2020; Grott et al., 2019, 2021; Spohn et al., 2018). The Phoenix measurements in Vastitas Borealis at 68.22°N 234.25°E, as well as the InSight measurements in Elysium Planitia at 4.50°N, 135.62°E, both showed that the martian soil is a poor thermal conductor. Thermal conductivity at the Phoenix site was determined to be 0.085 W m^{-1} K^{-1} in the upper 1.5 cm of the soil (Zent et al., 2010), while an average thermal conductivity of 0.039 ± 0.002 W m^{-1} K^{-1} was determined for the upper 37 cm of the soil column at the InSight landing site (Grott et al., 2021). As grain sizes at the two landing sites are comparable (Goetz et al., 2010; Grott et al., 2021; Presley & Christensen, 1997), similar thermal conductivities would be expected, and the difference between the two measurements has been attributed to the presence of cementing agents like perchlorate salts (Grott et al., 2021), which are abundant at the polar Phoenix landing site (Hecht et al., 2009; Kounaves, Carrier, et al., 2014). However, perchlorates may also be present at InSight (Navarro-González et al., 2010; Glavin et al., 2013; Kounaves, Chaniotakis, et al., 2014). Therefore, it seems likely that the presence of ground ice near the surface (Mellon et al., 2009) and the resulting atmospheric water vapor interactions (Fischer et al., 2019) may play an important role in increasing soil thermal conductivity at the Phoenix site when compared to the results presented here. To study the relative importance of grain-to-grain as well as gas conduction in the martian soil, measurements at different atmospheric pressures are needed. However, due to the Phoenix mission's limited lifetime, such measurements could not be made. Here we report on the first long term monitoring of soil thermal conductivity as a function of atmospheric pressure as derived from in situ measurements at the InSight landing site.

2. Probe Emplacement, Data Acquisition, and Inversion

The HP^3 mole is a self penetrating probe with a length of 400 mm and a diameter of 27 mm that uses a hammering mechanism to achieve soil penetration. Heating foils inside the mole allow the probe to be used as a modified line heat source. Following deployment onto the martian surface, HP^3 started its first penetration attempt on Sol 92 of the mission (28 February 2019). However, insufficient friction to compensate for recoil during hammering resulted in an initial failure to penetrate (Spohn, Hudson, Marteau, et al., 2022; Spohn, Hudson, Witte, et al., 2022). Further penetration was only possible after removing the HP^3 support structure and using the lander's robotic arm to provide friction by directly interacting with the HP^3 mole. In this way, it was possible to reach a mole depth of approximately 3 cm below the surface as measured from the mole's back cap. Following penetration, the hole behind the mole was filled with scraped soil which was tamped down to ensure that the mole was fully buried and in contact with soil. A first thermal conductivity measurement with a fully buried mole was conducted on Sol 680 of the mission and a final hammering attempt was conducted on Sol 754. However, no additional depth progress was observed and further penetration attempts were abandoned.

The final burial of the HP^3 mole is shown in Figure 1a and thermal conductivity was measured in this configuration when energy could be made available on the lander. Six measurements were conducted on Sols 798, 827, 874, 1070, 1160, and 1204, corresponding to solar longitudes L_s of 8.0°, 22.0°, 44.2°, 135.3°, 184.0°, and 210.0°, where L_s is defined as the aerocentric longitude measured from the northern hemisphere spring equinox where $L_s = 0°$. During the measurements, the mole was used as a modified line heat source (Hammerschmidt & Sabuga, 2000; Spohn et al., 2018) and a specified constant heating power was provided to the mole's outer hull. Thermal conductivity was then determined from the resulting temperature rise of the mole hull as a function of time (Spohn et al., 2018). Before each active heating experiment was started, background temperature drift was monitored for 2 Sols and the average was subtracted from the measurements to obtain the heating-induced temperature rise from which conductivity was determined (see Grott et al. (2021) for details).

A schematic cross section of the soil surrounding the mole, which has been derived based on geologic observations (Golombek, Williams, et al., 2020) and the history of probe emplacement (Spohn, Hudson, Marteau, et al., 2022), is shown in Figure 1b. It includes a layer of unconsolidated surficial dust and sand as well as a hole surrounding the back of the mole, which has been back-filled by scraping unconsolidated material followed by tapping the soil down using the robotic arm's scoop. Furthermore, a duricrust, whose presence is inferred from image and penetration data and that is underlying the unconsolidated material, is indicated. At larger depth,

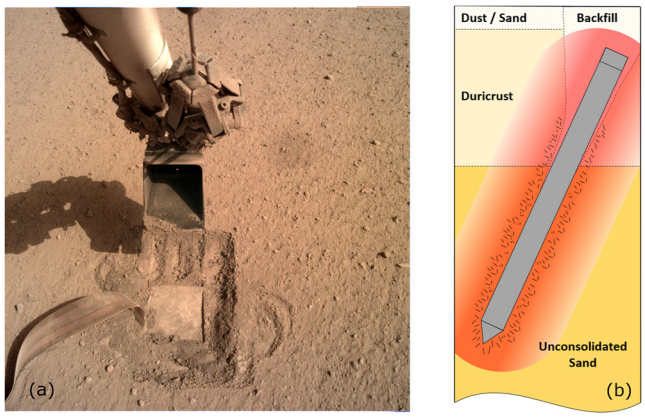

Figure 1. (a) Configuration of the HP^3 mole after the final penetration attempts on Sol 754 of the mission. During final hammering, the robotic arm's scoop pressed onto the ground (note the smooth rectangular imprint) to provide support and increase pressure on the mole hull. The scoop also acted as a safeguard to prevent the mole from recoiling backwards. The image was taken after retraction of the robotic arm on Sol 755. For reference, the width of the scoop and the extent of its imprint on the soil are about 7 cm. (b) Schematic cross section of the soil surrounding the mole indicating a surficial dust and sand layer over a duricrust and unconsolidated sand. The hole around the back of the mole was back-filled with unconsolidated material and tamped down. The volume of soil sampled by the thermal conductivity experiments as well as the region of potentially disrupted soil is indicated. The back cap of the mole is approximately 3 cm below the surface while the mole tip reached a depth of approximately 37 cm.

the soil is inferred to be unconsolidated. The soil volume sampled by the experiments is indicated in red shades and the generated heat pulse has a diffusion length scale of $d_\epsilon = \sqrt{kt/\rho c_p}$. Assuming a thermal conductivity of $k = 0.0385$ W m^{-1} K^{-1}, density ρ of 1,211 kg m^{-3}, and heat capacity c_p of 630 J kg^{-1} K^{-1}, $d_\epsilon \approx 6.2$ cm for the 21 hr 40 min heating experiment. The volume of soil sampled during the experiment extends to 2–3 mol diameters and is thus considerably larger than the region of potentially disrupted soil (also compare Figure 3 in Grott et al. (2021)). Note that the presence of a gravel layer around of the tip of the mole has been hypothesized based on the mole's penetration performance (Spohn, Hudson, Marteau, et al., 2022) but is not shown here. The tilt of the mole with respect to the local gravity vector is close to 30°.

The retrieved temperature rise as a function of time t is shown for all six thermal conductivity measurements in Figure 2 and all measurements were performed in the final mole configuration with no hammering in between. Heating curves followed a similar trend, showing the classical log-linear increase of temperature as a function of $\log(t)$ at intermediate heating times between 2 and 10 hr before axial heat flow causes a deviation at later times.

For a classical line heat source, the slope of the heating curve $dT/d\log(t)$ is inversely proportional to the thermal conductivity of the medium. Therefore a first qualitative conclusion concerning the pressure dependence of thermal conductivity at the InSight landing site can be already drawn from inspection of the slopes in Figure 2. In the figure, large slopes are associated with Sols of low atmospheric pressure and vice versa (compare Table 1), which implies that soil thermal conductivity and atmospheric pressure are positively correlated. This conclusion is supported by analytical models (Carslaw & Jaeger, 1959; Hammerschmidt & Sabuga, 2000; Jaeger, 1956) and a linear analysis roughly reproduces the trends reported below (see Supporting Information S1). However, using the classical line heat source approach (von Herzen & Maxwell, 1959), thermal conductivities are slightly overestimated due to the fact that axial heat flow cannot be accounted for in these models (Blackwell, 1956).

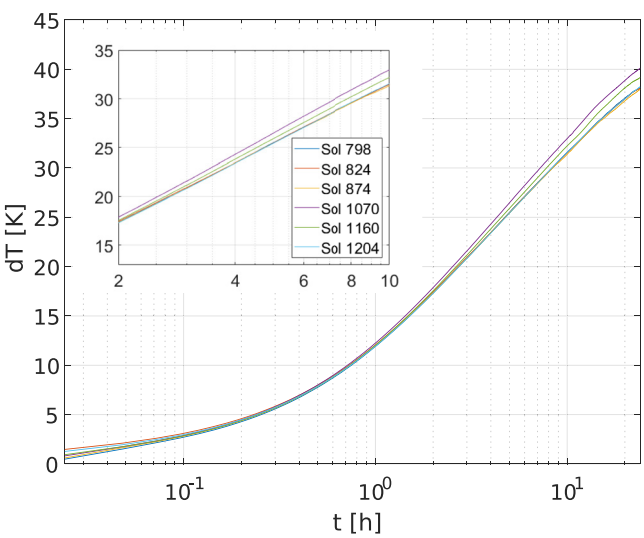

Figure 2. Temperature rise as a function of heating time t for all measurements performed in the fully buried, final mole configuration. The inset shows details of the log-linear regime between 2 and 10 hr after the start of the measurements.

Therefore, we rely on numerical models to invert the heating curves for soil thermal conductivity k. The model accounts for the non-negligible specific heat of the mole, the contact conductance H between mole and regolith as well as the geometry of the problem including axial heat transport. It is described in detail in Spohn et al. (2018) and Grott et al. (2019, 2021), and we used a Monte-Carlo approach to find admissible sets of model parameters k and H which fit the observations. While thermal conductivity k as well as contact conductance H change as a function of atmospheric pressure, soil density ρ remains unaffected and we require the numerical model to fit measurements at different seasons using a fixed density.

For each model run, modeled temperature $T_{\mathrm{mod}}(t, k, H)$ is compared to the measured temperature rise $T_{dat}(t)$ and the root mean square deviation between the two quantities is determined according to

$$\Delta T_{rms}(k, H) = \left(\sum_{i=1}^{n} \left(T_{\mathrm{mod}}(t_i, k, H) - T_{dat}(t_i)\right)^2 / n \right)^{\frac{1}{2}} \quad (1)$$

here $n = 1{,}000$ is the number of measurement points. Following Grott et al. (2021), data were inverted between $t_1 = 1$ hr and $t_n = 21$ hr 40 min. Admissible parameter sets (k, H) were then determined by requiring the root mean square deviation $\Delta T_{rms}(k, H)$ to be smaller than 0.17 K. This threshold takes the observed day-to-day temperature variations as well as other sources

Table 1
Summary of Thermal Conductivity Measurements Performed by the HP³ Instrument in the Final Measurement Configuration Following Sol 754

Sol	L_s [°]	T_0 [K]	P_{avr} [mbar]	P_{min} [mbar]	P_{max} [mbar]	ρ [kg m^{-3}]	k [W m^{-1} K^{-1}]
798	8.0	222.02	7.30	7.07	7.52	1,211	0.0388 ± 0.0009
827	22.0	220.26	7.44	7.20	7.65	1,211	0.0392 ± 0.0006
874	44.2	217.75	7.61	7.39	7.75	1,211	0.0395 ± 0.0006
1070	135.3	218.61	6.39	6.21	6.53	1,211	0.0367 ± 0.0009
1160	184.0	225.37	6.60	6.35	6.89	1,211	0.0371 ± 0.0007
1204	210.0	226.83	7.20	6.96	7.40	1,211	0.0389 ± 0.0007
798	8.0	222.02	7.30	7.07	7.52	1,007	0.0383 ± 0.0007
827	22.0	220.26	7.44	7.20	7.65	1,007	0.0395 ± 0.0007
874	44.2	217.75	7.61	7.39	7.75	1,007	0.0397 ± 0.0007
1070	135.3	218.61	6.39	6.21	6.53	1,007	0.0366 ± 0.0007
1160	184.0	225.37	6.60	6.35	6.89	1,007	0.0371 ± 0.0006
1204	210.0	226.83	7.20	6.96	7.40	1,007	0.0390 ± 0.0008

Note.The mission Sol number, the corresponding martian solar longitude (L_s), soil temperature at the beginning of the experiment T_0, average (P_{avr}), minimum (P_{min}) and maximum (P_{max}) atmospheric pressure during the measurement, as well as the assumed soil density ρ are given together with the determined thermal conductivity k. Chosen densities of 1,211 and 1,007 kg m^{-3} correspond to estimates that include and do not include an additional constraint posed by the surface thermal inertia (Grott et al., 2021), respectively. Stated error bars represent 1-σ confidence intervals.

of uncertainty into account (see Grott et al. (2021) for details). As the soil density was not known a priori, we ran two different sets of inversions using the two median densities derived for the InSight landing site by Grott et al. (2019). These are ρ = 1,007 kg m^{-3} and ρ = 1,211 kg m^{-3}, where the latter corresponds to an estimate that includes the additional constraint posed by the surface thermal inertia as derived from HP^3 radiometer measurements (N. T. Mueller et al., 2020; N. Mueller et al., 2021). For the soil specific heat capacity, a value of 630 J kg^{-1} K^{-1} has been assumed (Morgan et al., 2018). Twenty thousand Monte-Carlo simulations were then run for each of the measurements performed on Sol 798, 827, 874, 1070, 1160, and 1204. In the simulations, thermal conductivity k and contact conductance H were drawn from uniform probability distributions spanning the range $0.034 < k < 0.042$ W m^{-1} K^{-1} and $3 < H < 250$ W m^{-2} K^{-1}, respectively.

A discussion of measurement uncertainty associated with the determination of thermal conductivity from HP^3 measurements is given in Grott et al. (2019) and Grott et al. (2021). However, for the present analysis, we are searching for relative changes in thermal conductivity only, such that systematic sources of uncertainty which are identical for all measurements can be neglected. These include the uncertainties associated with determining the heat input into the TEM-A foils, the uncertainty associated with the imperfections of the finite element model, as well as the uncertainty of the reference method (Grott et al., 2021). Only the contribution stemming from the allowable spread of models determined using the Monte-Carlo simulations needs to be considered, and error bars stated below refer to the 1-σ standard deviations of the admissible model parameters.

Atmospheric pressure at the InSight Landing site has been measured at a cadence of 20 Hz by the Pressure Sensor (PS) of the InSight Auxiliary Payload Sensor Suite (APSS) (Banfield et al., 2019, 2020; Spiga et al., 2018), and we here use the most recent recalibrated data set as provided by Lange et al. (2022). Diurnal average surface atmospheric pressure P can be approximated by

$$P = a_0 + \sum_{n=1}^{6} a_n \cos(nL_s) + b_n \sin(nL_s) \quad (2)$$

where the coefficients are given in units of Pascals and a_0 = 721.5, a_1 = 36.99, a_2 = −34.57, a_3 = −0.6312, a_4 = −0.3281, a_5 = 0.1213, a_6 = 0.6940, b_1 = −33.99, b_2 = 36.77, b_3 = −0.6382, b_4 = −3.655, b_5 = 0.6656, and b_6 = 0.8195. L_s is solar longitude in degrees. Average diurnal atmospheric pressure at the landing site is thus found to vary between 6.25 and 7.95 mbar.

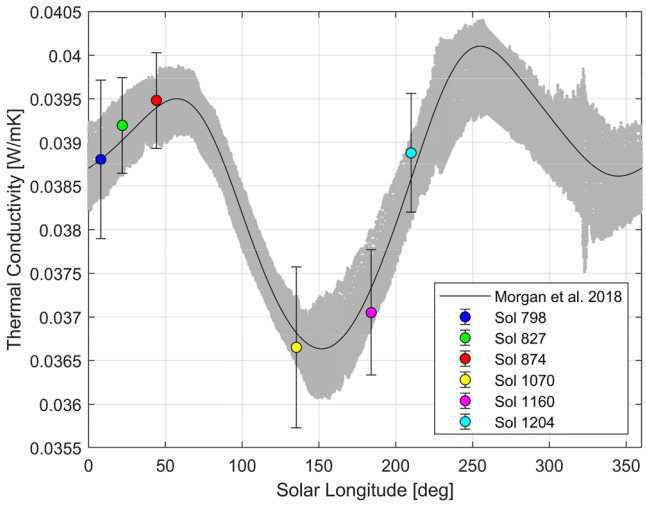

Figure 3. Thermal conductivity as a function of martian season assuming $\rho = 1{,}211$ kg m^{-3}. Six active heating experiments were conducted over the period of $L_s = 8.0°$ to $L_s = 210°$ before the reduction of solar power on the InSight lander prevented further measurements to be taken toward the end of the mission. A model of thermal conductivity as a function of atmospheric pressure is shown for reference (Morgan et al., 2018), where we have fixed k_0 (compare Equation 3) to correspond to the Sol 798 measurement. Here, the solid line corresponds to average diurnal atmospheric pressures and the gray shaded area shows the expected range of thermal conductivities encountered during each Sol. Error bars refer to the 1-σ standard deviations of the admissible thermal conductivities as derived from Monte-Carlo simulations. They do not include systematic sources of uncertainty, which are identical for all measurements (see text for details).

Soil thermal conductivity corresponding to the above atmospheric pressures can be estimated using the model of Morgan et al. (2018), which is based on a parameterization of laboratory experiments on unconsolidated soil performed by Presley and Christensen (1997). Given the soil thermal conductivity $k_0(P)$ at atmospheric pressure P, thermal conductivity at pressure $P + \Delta P$ can be calculated from

$$k(P + \Delta P) = k_0(P)\left(1 + A\Delta P + B\Delta P^2\right) \quad (3)$$

where ΔP is the atmospheric pressure deviation with respect to P in mbar. The fitting constants A and B are given by 5.173 mbar^{-1} and -0.2416 mbar^{-2}, respectively (Morgan et al., 2018).

3. Results

Results of the simulations are summarized in Table 1, where the Sol number, martian solar longitude L_s, soil temperature at the beginning of the experiment T_0, average (P_{avr}), minimum (P_{min}) and maximum (P_{max}) atmospheric pressure during the measurement, as well as soil density ρ are given together with the derived thermal conductivity k. A clear correlation between atmospheric pressure and soil thermal conductivity is evident. Results are insensitive to the chosen soil density, and derived soil thermal conductivities for the two sets of simulations using $\rho = 1{,}007$ kg m^{-3} and $\rho = 1{,}211$ kg m^{-3} are indistinguishable within their respective error bars. Note that in principle the temperature dependence of heat capacity and soil matrix thermal conductivity could account for some of the seasonal variations observed in the inverted thermal conductivities. However, because there is no correlation between soil temperature T_0 and thermal conductivity k in Table 1, such an effect can be ruled out. Also, a direct influence of the observed seasonal trend on the variations of seismic velocities as reported by Compaire et al. (2022) is unlikely for the same reason.

Soil thermal conductivity for the case $\rho = 1{,}211$ kg m^{-3} is shown in Figure 3 as a function of martian solar longitude L_s for the measurements taken on sols 798, 827, 874, 1070, 1160 and 1204, corresponding to $L_s = 8.0°$, 22.0°, 44.2°, 135.3° 184.0°, and 210.0°, respectively. Measurements roughly span ~60% of a martian year while covering ~85% of the encountered pressures. To compare the obtained results with conductivities expected for unconsolidated soils, we have converted average diurnal atmospheric pressure for each measurement to a thermal conductivity estimate using Equation 3. Choosing the thermal conductivity derived for Sol 798 to fix $k_0(P)$, soil thermal conductivity can be estimated as a function of L_s by first calculating the average diurnal atmospheric pressure using Equation 2, and then calculating the expected conductivity change with respect to $k_0(P)$ using Equation 3. The result of this calculation is shown as the solid line in Figure 3 (Morgan et al., 2018). In addition, the gray-shaded area corresponds to the range of conductivities predicted including the diurnal pressure fluctuations. As is evident from the figure, the measured soil thermal conductivities closely follow model predictions, indicating that there is a clear positive correlation of thermal conductivity and atmospheric pressure, that is, increased atmospheric pressure results in increased soil thermal conductivity and vice versa.

4. Discussion

We have conducted the first long-term in situ monitoring of martian soil thermal conductivity using the HP^3 mole as a modified line heat source. We find that soil thermal conductivity at the InSight landing site correlates with atmospheric pressure and follows the trend predicted by laboratory experiments for unconsolidated soils (Presley & Christensen, 1997). For the conducted experiments, pressure variations of 1.2 mbar resulted in conductivity changes of close to 8%, corresponding to approximately 6.5% mbar^{-1}. These changes are consistent with model predictions and indicate that a significant fraction of heat transport occurs through the pore-filling gas. Note, that although relative humidity follows a trend similar to the annual pressure fluctuations discussed here (Pal &

Kereszturi, 2020), the very low partial pressure of water vapor is unlikely to have a noticeable effect on our measurements. While water capillary bridges can dominate the heat transfer in granular material (Persson, 2023), these are not expected to be present for extended periods of time at the InSight landing site (Pal & Kereszturi, 2020).

Any cementation or induration of the soil would have a significant influence on thermal properties by increasing the contact area between individual grains (Piqueux & Christensen, 2009a) and this does not seem to be the case for the soil sampled by the HP^3 mole. Even small amounts of cement would result in a significant increase of heat transport through the grain matrix and the pressure dependence of thermal conductivity would be minimal (Piqueux & Christensen, 2009b). Therefore, thermal measurements indicate that the sampled soil is unconsolidated.

Some support for the conclusion that soil cementation should be minimal is provided by the analysis of seismic velocities in the shallow subsurface. Using the HP^3 hammering mechanism as a seismic source, Brinkman et al. (2022) determined P-wave v_P and S-wave v_S velocities in the upper few tens of centimeters of the soil. They found velocities of $v_P = 119^{+45}_{-21}$ and $v_S = 63^{+11}_{-7}$ m s^{-1}, consistent with values typically encountered in low-density unconsolidated sands. Furthermore, Wright et al. (2022) suggested that any cement at grain contacts within sediment layers at the InSight landing site may have been broken up by impacts or marsquakes, although this may be more relevant for deeper soil layers not probed by the HP^3 mole.

Nagihara et al. (2022) studied the dependence of thermal conductivity on atmospheric pressure in the lab using the low-cohesion Mojave Mars simulant (Peters et al., 2008) as an analogue for the martian soil. The simulant is made from crushed basalt with grain sizes ranging from 0.05 to 1 mm and a median grain size of 0.2 mm, slightly larger but comparable to the values derived for the landing site (Grott et al., 2021). Cohesion of the simulant is low and smaller than 2 kPa. Experiments were conducted at two different soil densities of 1,540 and 1,660 kg m^{-3} and atmospheric pressure was varied between 2 and 10 mbar. While absolute thermal conductivity of the simulant was larger than that determined for the soil at the InSight landing site, which may be attributed to the larger grain sizes and larger density of the simulant when compared to the in situ measurements, Nagihara et al. (2022) found the pressure dependence of thermal conductivity to be similar to the one reported here. Over a pressure range of 6–10 mbar, the simulant's thermal conductivity increased by 20%, corresponding to 5% mbar^{-1} and thus being comparable to the 6.5% mbar^{-1} observed here.

At the InSight landing site, the thermally dominant grain size as derived from a comparison of soil thermal conductivity with results of laboratory experiments (Presley & Christensen, 1997) is close to 125 μm. As the largest particles dominate bulk thermal conductivity (Presley & Craddock, 2006), up to 95% of all particles in the soil sampled by the HP^3 experiment could be smaller than 125 μm. In particular, dust sized particles could be intermixed with larger grains. These small particles could add significant cohesion to the soil, which would help to explain the presence of steep sided pits in image data (Golombek, Warner, et al., 2020) as well as the lack of friction on the mole's outer hull during penetration (Spohn, Hudson, Witte, et al., 2022).

While thermal conductivity measurements thus clearly indicate that soil cementation or induration should be minimal, minimal cementation is difficult to reconcile with image data that show clods in the pits and on the surface (Golombek, Warner, et al., 2020) as well as with cohesion estimates that have been derived using the lander's robotic arm (Marteau et al., 2021). These data strongly suggest a duricrust to be present, which could have been generated by the deposition of salts due to soil-atmosphere interactions (Banin et al., 1992; Ditteon, 1982; Haskin et al., 2005; Hurowitz et al., 2006; Moore et al., 1999; Mutch et al., 1977). However, experimental studies have shown that granular materials behave more cohesively when tested under vacuum (Bromwell, 1966; Grossman et al., 1970; Salisbury et al., 1964) and reduced-gravity conditions (Elekes & Parteli, 2021; Kleinhans et al., 2011; Walton et al., 2007; White & Klein, 1990), which suggests an enhanced cohesive behavior of the soil under Martian atmospheric pressure and gravity. The penetration data gathered by the HP^3 mole also indicates significant penetration resistance of the soil (Spohn, Hudson, Marteau, et al., 2022).

This discrepancy may be resolved when considering the history of probe emplacement. During the initial penetration attempts, the soil was significantly disrupted and a hole up to 7 cm deep was created around the mole. This was later back-filled by loose material, but the duricrust in this depth range has been disaggregated into sand (Spohn, Hudson, Marteau, et al., 2022). At larger depth, some soil may also have been disrupted, but the amount of modified material is estimated to be minor when compared to the volume sampled by the heat pulse generated in the thermal conductivity experiments, which extends to approximately 2–3 mol diameters (see above).

Therefore, the soil properties derived here should correspond to the unconsolidated soil layers surrounding the mole at larger depths rather than the duricrust closer to the surface.

The existence of gas exchange between soil and the martian atmosphere has been inferred from models of the martian climate (e.g., Martínez et al. (2017); Buhler and Piqueux (2021)), models for regolith-water exchange (e.g., Savijärvi et al. (2016)), models for the transport of trace gases (e.g., Bullock et al. (1994)), as well as models for barometric pumping (de Beule et al., 2014). Furthermore, the exchange and adsorption of gases has been studied in the lab (e.g., Fanale, Banerdt, et al. (1982); Fanale, Salvail, et al. (1982); Rannou et al. (2001)). However, to our knowledge, the thermal conductivity data presented here is the first direct evidence that the atmosphere interacts with the top most meter of material on Mars.

5. Conclusions

Soil thermal conductivity at the InSight landing site strongly correlates with atmospheric pressure and conductivities vary by 6.5% $mbar^{-1}$. This is within the range predicted by models of thermal conductivity as a function of pressure for unconsolidated soils (Morgan et al., 2018) and consistent with the results of laboratory experiments under martian atmospheric conditions (Nagihara et al., 2022; Presley & Christensen, 1997). Furthermore, the observed strong correlation between thermal conductivity and atmospheric pressure indicates that pore spaces may be filled with dust sized particles, which could result in significant soil cohesion.

Both the rather low absolute value of thermal conductivity of around 0.038 W m^{-1} K^{-1} as well as the observed strong pressure dependence of 6.5% $mbar^{-1}$ indicate that the soil probed by the HP^3 experiment is unconsolidated. Cementation or induration would significantly increase grain-to-grain contacts and thus increase the absolute conductivity by a large factor while at the same time removing the pressure dependence (Piqueux & Christensen, 2009b). We conclude that the thermal properties derived here are representative for the deeper, unconsolidated soil layers rather than the undisturbed duricrust observed in image data.

Data Availability Statement

Calibrated HP^3 heating experiment data are archived in NASA's Planetary Data System (InSight HP3 Science Team, 2021). The numerical code and data necessary to reproduce the results and figures of this paper have been made publicly available in Grott (2022).

Acknowledgments
The design, building of and research into the HP^3 has been supported by the German Aerospace Center DLR, by NASA, the ÖAW, and the Polish Academy of Science. US government support is gratefully acknowledged. This research was carried out in part at the Jet Propulsion Laboratory, California Institute of Technology, under a contract with the National Aeronautics and Space Administration (80NM0018D0004). This paper is InSight Contribution Number 306. Open Access funding enabled and organized by Projekt DEAL.

References

Banerdt, W. B., Smrekar, S. E., Banfield, D., Giardini, D., Golombek, M., Johnson, C. L., et al. (2020). Initial results from the InSight mission on Mars. *Nature Geoscience*, *13*(3), 183–189. https://doi.org/10.1038/s41561-020-0544-y

Banfield, D., Rodriguez-Manfredi, J. A., Russell, C. T., Rowe, K. M., Leneman, D., Lai, H. R., et al. (2019). InSight Auxiliary Payload Sensor Suite (APSS). *Space Science Reviews*, *215*(1), 4. https://doi.org/10.1007/s11214-018-0570-x

Banfield, D., Spiga, A., Newman, C., Forget, F., Lemmon, M., Lorenz, R., et al. (2020). The atmosphere of Mars as observed by InSight. *Nature Geoscience*, *13*(3), 190–198. https://doi.org/10.1038/s41561-020-0534-0

Banin, A., Clark, B. C., & Waenke, H. (1992). Surface chemistry and mineralogy. In M. George (Ed.), *Mars* (pp. 594–625).

Blackwell, J. H. (1956). The axial-flow error in the thermal-conductivity probe. *Canadian Journal of Physics*, *34*(4), 412–417. https://doi.org/10.1139/p56-048

Brinkman, N., Schmelzbach, C., Sollberger, D., ten Pierick, J., Edme, P., Haag, T., et al. (2022). In-situ regolith seismic velocity measurement at the insight landing site on Mars. *Earth and Space Science Open Archive*, *32*. https://doi.org/10.1002/essoar.10512064.1

Bromwell, L. G. (1966). The friction of quartz in high vacuum (Tech. Rep. No. 3-101). Department of Civil Engineering, M.I.T. *Research in earth physics* Phase Report No. 7.

Buhler, P., & Piqueux, S. (2021). Obliquity-driven CO_2 exchange between Mars' atmosphere, regolith, and polar cap. *Journal of Geophysical Research: Planets*, *126*(5). https://doi.org/10.1029/2020JE006759

Bullock, M. A., Stoker, C. R., McKay, C. P., & Zent, A. P. (1994). A coupled soil-atmosphere model of H_2O_2 on Mars. *Icarus*, *107*(1), 142–154. https://doi.org/10.1006/icar.1994.1012

Carslaw, H., & Jaeger, J. (1959). *Conduction of heat in solids* (2nd ed., Vol. 13). Oxford at the Clarendon Press.

Compaire, N., Margerin, L., Monnereau, M., Garcia, R. F., Lange, L., Calvet, M., et al. (2022). Seasonal variations of subsurface seismic velocities monitored by the SEIS-InSight seismometer on Mars. *Geophysical Journal International*, *229*(2), 776–799. https://doi.org/10.1093/gji/ggab499

de Beule, C., Wurm, G., Kelling, T., Küpper, M., Jankowski, T., & Teiser, J. (2014). The martian soil as a planetary gas pump. *Nature Physics*, *10*(1), 17–20. https://doi.org/10.1038/nphys2821

Ditteon, R. (1982). Daily temperature variations on Mars. *Journal of Geophysical Research*, *87*(B12), 10197–10214. https://doi.org/10.1029/JB087iB12p10197

Edgett, K. S., Yingst, R. A., Minitti, M. E., Goetz, W., Kah, L. C., Kennedy, M. R., et al.MSL Science Team. (2013). Mars Hand Lens Imager (MAHLI) efforts and observations at the "Rocknest" Eolian sand shadow in curiosity's gale crater field Site. In *Lunar and planetary science conference* (p. 1201).

Elekes, F., & Parteli, E. J. R. (2021). An expression for the angle of repose of dry cohesive granular materials on Earth and in planetary environments. *Proceedings of the National Academy of Sciences of the United States of America*, *118*(38), e2107965118. https://doi.org/10.1073/pnas.2107965118

Fanale, F. P., Banerdt, W. B., Saunders, R. S., Johansen, L. A., & Salvail, J. R. (1982a). Seasonal carbon dioxide exchange between the regolith and atmosphere of Mars: Experimental and theoretical studies. *Journal of Geophysical Research*, *87*(B12), 10215–10225. https://doi.org/10.1029/JB087iB12p10215

Fanale, F. P., Salvail, J. R., Banerdt, W. B., & Saunders, R. S. (1982b). Mars: The regolith-atmosphere-cap system and climate change. *Icarus*, *50*(2–3), 381–407. https://doi.org/10.1016/0019-1035(82)90131-2

Fergason, R., Christensen, P., Bell, J., Golombek, M., Herkenhoff, K., & Kieffer, H. (2006). Physical properties of the Mars Exploration Rover landing sites as inferred from Mini-TES-derived thermal inertia. *Journal of Geophysical Research*, *111*(E2), E02S21. https://doi.org/10.1029/2005JE002583

Fischer, E., Martínez, G. M., Rennó, N. O., Tamppari, L. K., & Zent, A. P. (2019). Relative humidity on Mars: New results from the phoenix TECP sensor. *Journal of Geophysical Research: Planets*, *124*(11), 2780–2792. https://doi.org/10.1029/2019JE006080

Glavin, D. P., Freissinet, C., Miller, K. E., Eigenbrode, J. L., Brunner, A. E., Buch, A., et al. (2013). Evidence for perchlorates and the origin of chlorinated hydrocarbons detected by SAM at the Rocknest Aeolian deposit in Gale Crater. *Journal of Geophysical Research: Planets*, *118*(10), 1955–1973. https://doi.org/10.1002/jgre.20144

Goetz, W., Pike, W. T., Hviid, S. F., Madsen, M. B., Morris, R. V., Hecht, M. H., et al. (2010). Microscopy analysis of soils at the Phoenix landing site, Mars: Classification of soil particles and description of their optical and magnetic properties. *Journal of Geophysical Research*, *115*(E12), E00E22. https://doi.org/10.1029/2009JE003437

Golombek, M., Warner, N. H., Grant, J. A., Hauber, E., Ansan, V., Weitz, C. M., et al. (2020a). Geology of the InSight landing site on Mars. *Nature Communications*, *11*(1), 1014. https://doi.org/10.1038/s41467-020-14679-1

Golombek, M., Williams, N., Warner, N. H., Parker, T., Williams, M. G., Daubar, I., et al. (2020b). Location and setting of the Mars InSight lander, instruments, and landing site. *Earth and Space Science*, *7*(10), e01248. https://doi.org/10.1029/2020EA001248

Grossman, J. J., Ryan, J. A., Mukherjee, N. R., & Wegner, M. W. (1970). Micro-chemical, microphysical and adhesive properties of lunar material. *Geochimica et Cosmochimica Acta - Supplement*, *1*, 2171.

Grott, M. (2022). Supplementary material for "Seasonal variations of soil thermal conductivity at the InSight landing site". *Figshare Collection*. https://doi.org/10.6084/m9.figshare.c.6359816

Grott, M., Spohn, T., Knollenberg, J., Krause, C., Hudson, T. L., Piqueux, S., et al. (2021). Thermal conductivity of the martian soil at the InSight landing site from HP^3 active heating experiments. *Journal of Geophysical Research: Planets*, *126*(7), e06861. https://doi.org/10.1029/2021JE006861

Grott, M., Spohn, T., Knollenberg, J., Krause, C., Scharringhausen, M., Wippermann, T., et al. (2019). Calibration of the heat flow and physical properties package (HP^3) for the InSight Mars mission. *Earth and Space Science*, *6*(12), 2556–2574. https://doi.org/10.1029/2019EA000670

Hamilton, V. E., Vasavada, A. R., Sebastián, E., Torre Juárez, M., Ramos, M., Armiens, C., et al. (2014). Observations and preliminary science results from the first 100 sols of MSL Rover Environmental Monitoring Station ground temperature sensor measurements at Gale Crater. *Journal of Geophysical Research: Planets*, *119*(4), 745–770. https://doi.org/10.1002/2013JE004520

Hammerschmidt, U., & Sabuga, W. (2000). Transient hot wire (THW) method: Uncertainty assessment. *International Journal of Thermophysics*, *21*(6), 1225–1278.

Haskin, L. A., Wang, A., Jolliff, B. L., McSween, H. Y., Clark, B. C., Des Marais, D. J., et al. (2005). Water alteration of rocks and soils on Mars at the Spirit rover site in Gusev crater. *Nature*, *436*(7047), 66–69. https://doi.org/10.1038/nature03640

Hecht, M. H., Kounaves, S. P., Quinn, R. C., West, S. J., Young, S. M. M., Ming, D. W., et al. (2009). Detection of perchlorate and the soluble chemistry of martian soil at the phoenix lander site. *Science*, *325*(5936), 64–67. https://doi.org/10.1126/science.1172466

Huetter, E. S., Koemle, N. I., Kargl, G., & Kaufmann, E. (2008). Determination of the effective thermal conductivity of granular materials under varying pressure conditions. *Journal of Geophysical Research*, *113*(E12), E12004. https://doi.org/10.1029/2008JE003085

Hurowitz, J. A., McLennan, S. M., Tosca, N. J., Arvidson, R. E., Michalski, J. R., Ming, D. W., et al. (2006). In situ and experimental evidence for acidic weathering of rocks and soils on Mars. *Journal of Geophysical Research*, *111*(E2), E02S19. https://doi.org/10.1029/2005JE002515

InSight HP3 Science Team. (2021). Mars InSight lander HP^3 data archive. *Planetary Data System*. https://doi.org/10.17189/1517573

Jaeger, J. C. (1956). Conduction of heat in an infinite region bounded internally by a circular cylinder of a perfect conductor. *Australian Journal of Physics*, *9*(2), 167. https://doi.org/10.1071/PH560167

Kleinhans, M. G., Markies, H., de Vet, S. J., In't Veld, A. C., & Postema, F. N. (2011). Static and dynamic angles of repose in loose granular materials under reduced gravity. *Journal of Geophysical Research*, *116*(E11), E11004. https://doi.org/10.1029/2011JE003865

Kounaves, S. P., Carrier, B. L., O'Neil, G. D., Stroble, S. T., & Claire, M. W. (2014). Evidence of martian perchlorate, chlorate, and nitrate in Mars meteorite EETA79001: Implications for oxidants and organics. *Icarus*, *229*, 206–213. https://doi.org/10.1016/j.icarus.2013.11.012

Kounaves, S. P., Chaniotakis, N. A., Chevrier, V. F., Carrier, B. L., Folds, K. E., Hansen, V. M., et al. (2014). Identification of the perchlorate parent salts at the Phoenix Mars landing site and possible implications. *Icarus*, *232*, 226–231. https://doi.org/10.1016/j.icarus.2014.01.016

Lange, L., Forget, F., Banfield, D., Wolff, M., Spiga, A., Millour, E., et al. (2022). InSight pressure data recalibration, and its application to the study of long-term pressure changes on Mars. *Journal of Geophysical Research: Planets*, *127*(5), e07190. https://doi.org/10.1029/2022JE007190

Marteau, E., Golombek, M., Vrettos, C., & Garvin, J. (2021). Soil mechanical properties at the InSight landing site on Mars. In *Lunar and planetary science conference* (p. 2067).

Martínez, G. M., Newman, C. N., De Vicente-Retortillo, A., Fischer, E., Renno, N. O., Richardson, M. I., et al. (2017). The modern near-surface martian climate: A review of in-situ meteorological data from Viking to curiosity. *Space Science Reviews*, *212*(1–2), 295–338. https://doi.org/10.1007/s11214-017-0360-x

Mellon, M. T., Arvidson, R. E., Sizemore, H. G., Searls, M. L., Blaney, D. L., Cull, S., et al. (2009). Ground ice at the phoenix landing site: Stability state and origin. *Journal of Geophysical Research*, *114*(E1), E00E07. https://doi.org/10.1029/2009JE003417

Moore, H. J., Bickler, D. B., Crisp, J. A., Eisen, H. J., Gensler, J. A., Haldemann, A. F. C., et al. (1999). Soil-like deposits observed by Sojourner, the Pathfinder rover. *Journal of Geophysical Research*, *104*(E4), 8729–8746. https://doi.org/10.1029/1998JE900005

Morgan, P., Grott, M., Knapmeyer-Endrun, B., Golombek, M., Delage, P., Lognonné, P., et al. (2018). A pre-landing assessment of regolith properties at the InSight landing site. *Space Science Reviews*, *214*(6), 104. https://doi.org/10.1007/s11214-018-0537-y

Mueller, N., Piqueux, S., Lemmon, M., Maki, J., Lorenz, R. D., Grott, M., et al. (2021). Near surface properties of martian regolith derived from InSight HP^3-RAD temperature observations during phobos transits. *Geophysical Research Letters*, *48*(15), e93542. https://doi.org/10.1029/2021GL093542

Mueller, N. T., Knollenberg, J., Grott, M., Kopp, E., Walter, I., Krause, C., et al. (2020). Calibration of the HP^3 radiometer on InSight. *Earth and Space Science*, *7*(5), e01086. https://doi.org/10.1029/2020EA001086

Mutch, T. A., Arvidson, R. E., Binder, A. B., Guinness, E. A., & Morris, E. C. (1977). The geology of the Viking lander 2 site. *Journal of Geophysical Research*, *82*(B28), 4452–4467. https://doi.org/10.1029/JS082i028p04452

Nagihara, S., Ngo, P., & Grott, M. (2022). Thermal properties of the Mojave Mars regolith simulant in Mars-like atmospheric conditions. *International Journal of Thermophysics*, *43*(7), 98. https://doi.org/10.1007/s10765-022-03023-y

Navarro-González, R., Vargas, E., de la Rosa, J., Raga, A. C., & McKay, C. P. (2010). Reanalysis of the Viking results suggests perchlorate and organics at midlatitudes on Mars. *Journal of Geophysical Research*, *115*(E12), E12010. https://doi.org/10.1029/2010JE003599

Pal, B., & Kereszturi, A. (2020). Annual and daily ideal periods for deliquescence at the landing site of insight based on GCM model calculations. *Icarus*, *340*, 113639. https://doi.org/10.1016/j.icarus.2020.113639

Persson, B. (2023). Heat transfer in granular media consisting of particles in humid air at low confining pressure. *The European Physical Journal B*, *96*(14), 2386–2403. https://doi.org/10.1140/epjb/s10051-023-00483-5

Peters, G. H., Abbey, W., Bearman, G. H., Mungas, G. S., Smith, J. A., Anderson, R. C., et al. (2008). Mojave Mars simulant—Characterization of a new geologic Mars analog. *Icarus*, *197*(2), 470–479. https://doi.org/10.1016/j.icarus.2008.05.004

Pike, W. T., Staufer, U., Hecht, M. H., Goetz, W., Parrat, D., Sykulska-Lawrence, H., et al. (2011). Quantification of the dry history of the Martian soil inferred from in situ microscopy. *Geophysical Research Letters*, *38*(24), L24201. https://doi.org/10.1029/2011GL049896

Piqueux, S., & Christensen, P. R. (2009a). A model of thermal conductivity for planetary soils: 1. Theory for unconsolidated soils. *Journal of Geophysical Research*, *114*(E9), E09005. https://doi.org/10.1029/2008JE003308

Piqueux, S., & Christensen, P. R. (2009b). A model of thermal conductivity for planetary soils: 2. Theory for cemented soils. *Journal of Geophysical Research*, *114*(E9), E09006. https://doi.org/10.1029/2008JE003309

Presley, M. A., & Christensen, P. R. (1997). Thermal conductivity measurements of particulate materials 2. Results. *Journal of Geophysical Research*, *102*(E3), 6551–6566. https://doi.org/10.1029/96JE03303

Presley, M. A., & Craddock, R. A. (2006). Thermal conductivity measurements of particulate materials: 3. Natural samples and mixtures of particle sizes. *Journal of Geophysical Research*, *111*(E9), E09013. https://doi.org/10.1029/2006JE002706

Presley, M. A., Craddock, R. A., & Zolotova, N. (2009). The effect of salt crust on the thermal conductivity of one sample of fluvial particulate materials under Martian atmospheric pressures. *Journal of Geophysical Research*, *114*(E11), E11007. https://doi.org/10.1029/2009JE003355

Rannou, P., Chassefière, E., Encrenaz, T., Erard, S., Génin, J., Ingrin, J., et al. (2001). Exocam: Mars in a box to simulate soil-atmosphere interactions. *Advances in Space Research*, *27*(2), 189–193. https://doi.org/10.1016/S0273-1177(01)00046-1

Salisbury, J. W., Glaser, P. E., Stein, B. A., & Vonnegut, B. (1964). Adhesive behavior of silicate powders in ultrahigh vacuum. *Journal of Geophysical Research*, *69*(2), 235–242. https://doi.org/10.1029/JZ069i002p00235

Savijärvi, H., Harri, A.-M., & Kemppinen, O. (2016). The diurnal water cycle at Curiosity: Role of exchange with the regolith. *Icarus*, *265*, 63–69. https://doi.org/10.1016/j.icarus.2015.10.008

Spiga, A., Banfield, D., Teanby, N. A., Forget, F., Lucas, A., Kenda, B., et al. (2018). Atmospheric science with InSight. *Space Science Reviews*, *214*(7), 109. https://doi.org/10.1007/s11214-018-0543-0

Spohn, T., Grott, M., Smrekar, S. E., Knollenberg, J., Hudson, T. L., Krause, C., et al. (2018). The heat flow and physical properties package (HP^3) for the InSight mission. *Space Science Reviews*, *214*(5), 96. https://doi.org/10.1007/s11214-018-0531-4

Spohn, T., Hudson, T. L., Marteau, E., Golombek, M., Grott, M., Wippermann, T., et al. (2022). The InSight HP^3 Penetrator (Mole) on Mars: Soil properties derived from the penetration attempts and related activities. *Space Science Reviews*, *218*(8), 72. https://doi.org/10.1007/s11214-022-00941-z

Spohn, T., Hudson, T. L., Witte, L., Wippermann, T., Wisniewski, L., Kedziora, B., et al. (2022). The InSight-HP^3 mole on Mars: Lessons learned from attempts to penetrate to depth in the Martian soil. *Advances in Space Research*, *69*(8), 3140–3163. https://doi.org/10.1016/j.asr.2022.02.009

von Herzen, R., & Maxwell, A. E. (1959). The measurement of thermal conductivity of deep-sea sediments by a needle-probe method. *Journal of Geophysical Research*, *64*(10), 1557–1563. https://doi.org/10.1029/JZ064i010p01557

Walton, O., De Moor, C., & Gill, K. (2007). Effects of gravity on cohesive behavior of fine powders: Implications for processing lunar regolith. *Granular Matter*, *9*(5), 353–363. https://doi.org/10.1007/s10035-006-0029-8

White, B. R., & Klein, S. P. (1990). Dynamic shear of granular material under variable gravity conditions. *AIAA Journal*, *28*(10), 1701–1702. https://doi.org/10.2514/3.10461

Wright, V., Dasent, J., Kilburn, R., & Manga, M. (2022). A minimally cemented shallow crust beneath insight. *Geophysical Research Letters*, *49*(15), e2022GL099250. https://doi.org/10.1029/2022GL099250

Yingst, R. A., Kah, L. C., Palucis, M., Williams, R. M. E., Garvin, J., Bridges, J. C., et al. (2013). Characteristics of pebble- and cobble-sized clasts along the Curiosity rover traverse from Bradbury Landing to Rocknest. *Journal of Geophysical Research: Planets*, *118*(11), 2361–2380. https://doi.org/10.1002/2013JE004435

Zent, A. P., Hecht, M. H., Cobos, D. R., Wood, S. E., Hudson, T. L., Milkovich, S. M., et al. (2010). Initial results from the thermal and electrical conductivity probe (TECP) on Phoenix. *Journal of Geophysical Research*, *115*(2), E00E14. https://doi.org/10.1029/2009JE003420